

Determination of the heart-to-mediastinum ratio of ^{123}I -MIBG uptake using dual-isotope (^{123}I -MIBG/ $^{99\text{m}}\text{Tc}$ -tetrofosmin) multi-pinhole CZT SPECT in patients with heart failure.

Tanguy Blaire^{1,2,3}, Alban Bailliez^{1,2,3}, Fayçal Ben Bouallegue⁴, Dimitri Bellevre⁵, Denis Agostini^{2,5}, Alain Manrique^{2,5}

¹ Department of Nuclear Medicine, UF 5881, Groupement des Hôpitaux de l'Institut Catholique de Lille, Lomme, France

² Normandie Univ, UNICAEN, Signalisation, électrophysiologie et imagerie des lésions d'ischémie-reperfusion myocardique, 14000 Caen, France

³ Department of Nuclear Medicine, IRIS, Polyclinique du Bois, Lille, France

⁴ Department of Nuclear Medicine, CHU de Montpellier, France

⁵ Department of Nuclear Medicine, CHU Cote de Nacre, Caen, France

Corresponding Author, scientist in training: Tanguy Blaire, MD, Department of Nuclear Medicine, UF 5881, Groupement des Hôpitaux de l'Institut Catholique de Lille, Lomme, France

Tel: (+33) 320 001 655, Fax: (+33) 320 098 010,

Email: Blaire.Tanguy@ghicl.net

Word counts: Abstract: 285 words; Article: 5029

Running title: ^{123}I -MIBG HMR using CZT SPECT

Financial support: No

ABSTRACT

The aim of this retrospective study was to determine the heart-to-mediastinum ratio (HMR) of ^{123}I -metaiodobenzylguanidine (MIBG) uptake obtained using a multi-pinhole cadmium-zinc-telluride (CZT)-based camera (Discovery NM 530c, DNM-530c, GE Healthcare, Milwaukee, WI, USA) in comparison with that obtained using conventional planar imaging (Infinia, GE Healthcare, Milwaukee, WI, USA). **Methods:** Forty consecutive heart failure patients underwent planar acquisition 4 h after ^{123}I -MIBG injection (191 ± 41 MBq). To localize the heart using DNM-530c, $^{99\text{m}}\text{Tc}$ -tetrofosmin (358 ± 177 MBq) was administered and a dual-isotope acquisition was performed. The HMRs were calculated (i) with conventional planar imaging ($\text{HMR}_{\text{planar}}$), (ii) with anterior reprojection images ($\text{HMR}_{\text{reproj}}$) and (iii) with transaxial reconstructed images using DNM-530c ($\text{HMR}_{\text{transaxial}}$). In a phantom study, we estimated a linear model fitting the CZT to the planar data that was further applied to provide corrected CZT HMR values in patients ($\text{cHMR}_{\text{reproj}}$ and $\text{cHMR}_{\text{transaxial}}$ respectively). **Results:** Thirty-four men and 6 women (71 ± 9 y/o) with ischemic (22 patients) and nonischemic (18 patients) heart failure completed the study. Twenty-two of the 40 patients (55%) were New York Heart Association class II, and ejection fraction was 35 ± 9 %. Compared to $\text{HMR}_{\text{planar}}$ (1.44 ± 0.14), $\text{HMR}_{\text{reproj}}$ (1.12 ± 0.19) and $\text{HMR}_{\text{transaxial}}$ (1.35 ± 0.34) were decreased ($p<0.0001$ and $p<0.01$ respectively). Corrected $\text{cHMR}_{\text{reproj}}$ (1.54 ± 0.09) and $\text{cHMR}_{\text{transaxial}}$ (1.45 ± 0.14) were different ($p<0.0001$). Lin's concordance correlation and Bland-Altman analysis demonstrated an almost perfect concordance and a high agreement between $\text{HMR}_{\text{planar}}$ and $\text{cHMR}_{\text{transaxial}}$ ($p=\text{NS}$) using transaxial reconstructed images but not with $\text{cHMR}_{\text{reproj}}$ using reprojection images ($p<0.0001$). **Conclusion:** This study demonstrated that determination of late HMR of cardiac ^{123}I -MIBG uptake using dual-isotope (^{123}I and $^{99\text{m}}\text{Tc}$) acquisition on a multi-pinhole CZT camera (DNM-530c) is feasible in patients with heart failure. However, this determination should be performed using transaxial reconstructed images and a linear correction based on phantom data acquisitions.

Keywords CZT, DNM-530c, MIBG, Heart-to-mediastinum ratio, heart failure, dual-isotope

INTRODUCTION

Impairment of cardiac sympathetic innervation assessed with ^{123}I -MIBG is recognized as an independent prognostic factor in patients with heart failure (1-6). The late HMR of ^{123}I -MIBG is a major predictor of sudden death and cardiac events in patients with heart failure. A HMR below 1.6 is associated with an increased risk. (6). Currently, the calculation of HMR requires a planar static image of the thorax. This technique is well-standardized and reproducible using a conventional Anger camera (7,8). Recently, dedicated cardiac single photon emission computed tomography (SPECT) cameras using CZT detectors have dramatically transformed the routine of myocardial perfusion imaging in patients with known or suspected coronary artery disease. These cameras have a better count detection sensitivity resulting in decreased acquisition times and injected radiopharmaceutical doses, and improved energy resolution, permitting better photon energy discrimination for dual-isotope imaging.

Myocardial perfusion imaging obtained using cardiac CZT cameras is well validated against the conventional Anger camera for the diagnosis of coronary artery disease (9-12). Only a few studies have evaluated myocardial sympathetic innervation imaging with these new generation detectors (13-16). With DNM-530c, Gimelli et al. (13,14) assessed regional left ventricular denervation, while D'Estanque et al. (15) reported the impact of scatter correction in dual-isotope ($^{201}\text{Tl}/^{123}\text{I}$ -MIBG) cardiac SPECT protocols for trigger zone assessment defined as areas of autonomic nervous system dysfunction in viable myocardium that may contribute to the genesis of ventricular arrhythmia. In the AdreCard study, Bellevre et al. (16) recently demonstrated that the determination of late HMR of ^{123}I -MIBG was feasible in patients with heart failure using a parallel collimator CZT camera (DSPECT, Biosensors International, Caesarea, Israel). The two commercially available CZT cameras differ for sensitivity (4-fold improved with DNM-530c, and nearly 7-fold with DSPECT), and spatial resolution (6.7 mm with DNM-530c, and 8.6 mm with DSPECT) leading to images with different sharpness and contrast-to-noise ratios (11,17,18). Until

now, there have been no reports on the use of the DNM-530c, a multi-pinhole CZT SPECT camera, for determining HMR of ^{123}I -MIBG uptake. As previously emphasized (19,20), quantification of HMR is influenced by the type of collimators used and the number of scattered photons. Consequently, the value of HMR is expected to depend on the type of CZT camera used, hence the need for a study to validate the multi-pinhole dedicated cardiac CZT camera.

The aim of this study was to compare the late HMR of ^{123}I -MIBG uptake determined using dual-isotope CZT acquisition (DNM-530c) with that determined using conventional planar imaging in patients with heart failure.

MATERIALS AND METHODS

Phantom Studies

To estimate the effectiveness of the DNM-530c camera in measuring HMR, we performed several phantom acquisitions using an anthropomorphic torso phantom (Data Spectrum, Hillsborough, NC) with a cardiac insert. The liver and mediastinum compartments were filled with 20 MBq (17.5 kBq/mL) and 5 MBq (0.6 kBq/mL) ^{123}I activities, respectively. Ten consecutive acquisitions were performed over 10 min using a conventional Anger camera (Infinia) and a CZT-camera (DNM-530c). The cardiac insert was repeatedly unloaded from 1.75 (11 kBq/mL), to 1.5, 1.25, 1.1, 0.94, 0.75, 0.5, 0.35, 0.25 and 0.1 MBq respectively to obtain a wide range of HMRs of ^{123}I , as previously described (16,20).

Patient Population

This retrospective study was approved by our Hospital Ethics Committee for Medical Research (CIER # 03/01/2016, France). Informed signed consent was obtained from all patients. Data from 40 consecutive patients with clinically stable ischemic or nonischemic heart failure (left ventricular ejection fraction, LVEF, <45 %) referred to our institution from May 2011 to May 2016, were retrospectively evaluated. Patients with a recent (<21 days) history of unstable angina or acute myocardial infarction were excluded from the study.

Conventional Anger Camera Protocol (Planar)

The imaging protocol (Figure 1) was performed according to the recommendations of the EANM Cardiovascular Committee and the European Council of Nuclear Cardiology (7). ^{123}I -MIBG (191±29 MBq depending on the patient's weight) was administered 30 min after blockade of the thyroid by oral administration of Lugol solution. Four hours after injection, the late planar image was first obtained on the conventional gamma camera system, a dual head gamma camera

(Infinia) equipped with low-energy high-resolution collimators. Planar images were acquired in the anterior view over 10 min (128×128 matrix), using a symmetric energy window (159 ± 10 keV).

Dual-isotope (^{123}I -MIBG/ $^{99\text{m}}\text{Tc}$ -tetrofosmin) CZT Acquisition Protocol (DNM-530c)

$^{99\text{m}}\text{Tc}$ -tetrofosmin (358 ± 177 MBq) was administered for myocardial perfusion imaging in order to localize the heart within the thorax. After 15 min, the $^{99\text{m}}\text{Tc}$ image helped to focus the detectors on the cardiac area. A 10-min list-mode simultaneous dual radionuclide ($^{99\text{m}}\text{Tc}$ and ^{123}I) gated scan was then performed using a dedicated CZT cardiac SPECT camera (DNM-530c). DNM-530c is equipped with 19 stationary CZT detectors, each equipped with a pinhole collimator, that simultaneously image 19 cardiac views, each detector being composed of four 5-mm-thick elements of 32×32 pixels (pixel size 2.46×2.46 mm) (17). List-mode acquisition permits the retrospective selection of $^{99\text{m}}\text{Tc}$ and ^{123}I energy windows, respectively set to 140 keV (-10 to +5 %) and 159 keV (-5 to +10 %). No scatter correction was performed. Previous studies using phantom data acquired separately for $^{99\text{m}}\text{Tc}$ and ^{123}I showed that $^{99\text{m}}\text{Tc}$ crosstalk into the ^{123}I window was negligible when performing a simultaneous CZT SPECT acquisition (21,22). To make sure that different $^{99\text{m}}\text{Tc}$: ^{123}I ratios do not impact on energy resolution, a set of energy spectra (single ^{123}I , single $^{99\text{m}}\text{Tc}$, dual ^{123}I - $^{99\text{m}}\text{Tc}$) was acquired using linear sources with three $^{99\text{m}}\text{Tc}$: ^{123}I ratios (0.5:1, 1:1, and 5:1), with a constant activity of ^{123}I (24 MBq) (see Figure 2).

Heart-to-mediastinum ^{123}I -MIBG Uptake Ratio (HMR) Analysis

A $\text{HMR}_{\text{planar}}$ was calculated on the planar images. Myocardial and mediastinal counts were obtained by drawing regions of interest (ROI) manually on the left ventricle and over the upper mediastinum area (7).

Using SPECT data, two different methods were tested for assessing the heart-to-

mediastinum ^{123}I -MIBG uptake ratio. First, a $\text{HMR}_{\text{reproj}}$ was calculated on a reprojected anterior view from the SPECT images reconstructed using the vendor's console. The reprojection of tomographic data assumed an ideal parallel hole collimation and did not simulate attenuation or scatter. A ROI encompassing the left ventricle was drawn manually on the $^{99\text{m}}\text{Tc}$ -tetrofosmin images and automatically copied to the ^{123}I -MIBG images. A mediastinum ROI (42 pixels) was then drawn on the ^{123}I -MIBG images.

Second, a $\text{HMR}_{\text{transaxial}}$ was calculated using the transaxial reconstructed SPECT images. A myocardial elliptic volume of interest (VOI) was drawn manually to encompass the whole heart on the $^{99\text{m}}\text{Tc}$ -tetrofosmin images. This VOI was automatically copied from the $^{99\text{m}}\text{Tc}$ -tetrofosmin images to the ^{123}I -MIBG images. A mediastinum VOI (300 voxels) was manually drawn on the ^{123}I -MIBG images.

Heart-to-mediastinum Ratio Correction Factor

Many factors affecting the HMR of ^{123}I -MIBG uptake differ between the Infinia and DNM-530c cameras, including the type of collimator (parallel-hole low-energy high-resolution with Infinia vs. multi-pinhole with DNM-530c), energy window, energy resolution which is better with DNM-530c (approximately 9% with Infinia vs. about 5% with DNM-530c), and detector material stopping power (84% for 9.5 mm NaI(Tl) vs. 78% for 5 mm CZT for 159 keV photons). To take into account the difference between DNM-530c and Infinia, a correction factor was applied to HMR quantification, based on phantom acquisitions. To extract a correction factor from the analysis, a linear regression equation obtained in the phantom study was used and the corrected- $\text{HMR}_{\text{reproj}}$ ($\text{cHMR}_{\text{reproj}}$) and the corrected- $\text{HMR}_{\text{transaxial}}$ ($\text{cHMR}_{\text{transaxial}}$) calculated for each patient in the validation group for further comparison with the $\text{HMR}_{\text{planar}}$ values (16,23).

LVEF $^{99\text{m}}\text{Tc}$ -tetrofosmin SPECT with DNM-530c

As previously reported (22), the presence of ^{123}I does not impact on LVEF assessment within the $^{99\text{m}}\text{Tc}$ energy window in the dual-isotope condition using DNM-530c. Accordingly, LVEF was assessed using Quantitative Gated SPECT software (QGS, Cedars-Sinai Medical Center, Los Angeles, CA).

Statistical Analysis

The normal distribution of data was tested with the Shapiro-Wilk test. Paired HMR values determined using Infinia and DNM-530c were compared using Student's t test for paired samples. Correlations between $\text{HMR}_{\text{planar}}$, $\text{HMR}_{\text{reproj}}$ and $\text{HMR}_{\text{transaxial}}$ were assessed using linear regression and Pearson's correlation. Concordance between $\text{HMR}_{\text{planar}}$, $\text{HMR}_{\text{reproj}}$ and $\text{HMR}_{\text{transaxial}}$ values was tested using Lin's concordance correlation coefficient (CCC) (24) and Bland-Altman analysis (25). Lin's CCC is essentially equivalent to the kappa coefficient but is applicable to continuous data. It evaluates both accuracy and precision, indicating how far the measurement pairs are away from the line of identity. Lin's CCC scale ranges from 0 (no agreement) to +1 (perfect agreement), where 0.21 – 0.40 indicates fair concordance, 0.41 – 0.60 moderate concordance, 0.61 – 0.80 substantial concordance and 0.81 – 1.00 almost perfect concordance. A two-tailed p value ≤ 0.05 was considered statistically significant. Statistical analysis was performed using R version 3.3.2 (R Foundation for Statistical Computing, Vienna, Austria).

RESULTS

Phantom Study

The HMR values obtained from the phantom acquisitions are listed in Table 1. The HMR_{reproj} (2.82 ± 1.5) and $HMR_{\text{transaxial}}$ (3.51 ± 1.94) were increased compared with HMR_{planar} (2.34 ± 0.8 , $p = \text{NS}$ and $p = 0.01$ respectively). However, Bland-Altman plots demonstrated that HMR_{reproj} and $HMR_{\text{transaxial}}$ values were underestimated for low HMR and overestimated for high HMR values. The corrections used for the calculation of $cHMR_{\text{reproj}}$ and $cHMR_{\text{transaxial}}$ were determined by linear regression between CZT and planar HMR in the phantom study: $cHMR_{\text{reproj}} = 0.4715 \times HMR_{\text{reproj}} + 1.0416$ ($r = 0.98$) and $cHMR_{\text{transaxial}} = 0.4106 \times HMR_{\text{transaxial}} + 0.8987$ ($r = 0.99$) respectively.

Population

Among the 40 consecutive patients (34 male, 6 female, mean age 71 ± 9 years, mean LVEF: $35\% \pm 9$) with heart failure included in the study, 22 (55%) had ischemic heart failure, and 18 (45%) had nonischemic heart failure. Patient characteristics are presented in Table 1. According to the New York Heart Association functional classification, 13 patients were class I, 22 class II, and 5 class III. End-diastolic and end-systolic volumes, and LVEF obtained using ^{99m}Tc -tetrofosmin SPECT were 171 ± 87 mL, 117 ± 67 mL and $36\% \pm 17$, respectively.

HMR Quantification in Patients: DNM-530c vs. Planar

In our population, the HMR_{reproj} (1.12 ± 0.19) and $HMR_{\text{transaxial}}$ (1.35 ± 0.34) were significantly lower than HMR_{planar} (1.44 ± 0.14 , $p < 0.0001$ and $p < 0.05$ respectively). Figures 3A and 4A show Lin's concordance correlation between HMR_{reproj} and HMR_{planar} (Figure 3A) and between $HMR_{\text{transaxial}}$ and HMR_{planar} (Figure 4A), and demonstrate only a fair concordance between HMR_{reproj} and HMR_{planar} ($\text{CCC} = 0.24$) and a substantial concordance between $HMR_{\text{transaxial}}$ and

HMR_{planar} (CCC= 0.61). Bland-Altman plots (Figure 3B and 4B) further demonstrated a poor agreement between HMR_{reproj} and HMR_{planar} (3B) and between $HMR_{\text{transaxial}}$ and HMR_{planar} (4B) leading to underestimation of values by DNM-530c. Figure 5 displays a case imaged with Infinia and DNM-530c.

HMR Quantification in Patients: Corrected DNM-530c vs. Planar

Corrected $cHMR_{\text{reproj}}$ (1.54 ± 0.09) but not $cHMR_{\text{transaxial}}$ (1.45 ± 0.14) was significantly higher than HMR_{planar} (1.44 ± 0.14 , $p < 0.0001$ and $p = \text{NS}$ respectively). As shown in Figure 3C, there was a moderate concordance between $cHMR_{\text{reproj}}$ and HMR_{planar} (CCC= 0.49) and Bland's Altman plots (Figure 3D) showed a moderate agreement between $cHMR_{\text{reproj}}$ and HMR_{planar} . The mean difference between the HMR values from the two techniques was 0.11, but significantly increased as a function of the mean HMR value.

In contrast, as shown in Figure 4C, there was an almost perfect concordance between $cHMR_{\text{transaxial}}$ and HMR_{planar} (CCC= 0.92). Bland's Altman plots (Figure 4D) showed high agreement between $cHMR_{\text{transaxial}}$ and HMR_{planar} values. The mean difference between the HMR values from the two techniques was 0.01, with a narrow 95 % confidence interval, and was stable over the whole range of HMR values.

DISCUSSION

Late HMR determination using the Anger camera is well standardized and its prognostic value is widely recognized. In this retrospective study, we determined the HMR of ^{123}I -MIBG uptake using a multi-pinhole dedicated cardiac CZT camera (DNM-530c) in patients with heart failure and low LVEF. To our knowledge, this is the first dual-isotope study combining ^{123}I -MIBG and $^{99\text{m}}\text{Tc}$ -tetrofosmin with a multi-pinhole CZT camera in order to assess cardiac neuronal function in heart failure. Late HMRs ($\text{HMR}_{\text{reproj}}$ and $\text{HMR}_{\text{transaxial}}$) were significantly lower in patients compared with planar imaging, but with high agreement with $\text{cHMR}_{\text{transaxial}}$. Our results are consistent with previous findings from the Adreca study (16) conducted using another model of the dedicated cardiac CZT camera with different spatial resolution and sensitivity (17,26).

Difference Between Planar and CZT SPECT HMR

Firstly, in order to better understand the camera responses in ^{123}I -MIBG imaging, we compared planar and DNM-530c phantom acquisitions, and found that the non-corrected HMRs obtained with the DNM-530c underestimated the low values and overestimated high values of ^{123}I -MIBG uptake. Accordingly, HMRs values in patients were significantly lower with the DNM-530c compared with the Anger camera, as these patients with heart failure had decreased ^{123}I -MIBG uptake.

The collimators used and the stopping power of the detector material may impact on the quantification of ^{123}I -MIBG HMR (20,27). Inoue et al. (23) found that a correction factor is necessary to improve exchangeability between the HMR values calculated using ME and low-to-medium energy collimators. Nakajima et al. demonstrated that the linear regression equation between low-energy and ME collimators obtained in a phantom study can be used for standardizing the measurement of HMR in ^{123}I -MIBG imaging (28-30). In our study, after

correction, there was still a significant difference between $\text{cHMR}_{\text{reproj}}$ and $\text{HMR}_{\text{planar}}$ ($p < 0.0001$), but there was no difference between $\text{cHMR}_{\text{transaxial}}$ and $\text{HMR}_{\text{planar}}$ ($p = \text{NS}$).

Using a different model of camera with mobile CZT detector columns and parallel tungsten collimators (DSPECT), Bellevre et al. extracted a planar equivalent image by projecting and summing all the elementary 2-D images that shared the same angle onto one large field of view virtual plane (16). After applying a similar correction based on linear regression between SPECT and planar phantom acquisitions, they found a high agreement between ^{123}I -MIBG HMR obtained using CZT and that obtained using planar imaging. In contrast, the moderate concordance between $\text{cHMR}_{\text{reproj}}$ and $\text{HMR}_{\text{planar}}$ we found using anterior reproj images is likely related to the multi-pinhole collimation, which is responsible for (i) a truncation artifact (31) that interferes with the mean counts of the myocardial ROI (see Figure 5) and for (ii) a larger non-uniformity with the DNM-530c compared with Anger camera (31). This limitation was overcome by using reconstructed transaxial images instead of reproj images for the measurement of corrected ^{123}I -MIBG HMR with the DNM-530c in our population.

Dual-isotope Acquisition

In our study, we performed simultaneous dual-isotope DNM-530c acquisitions with $^{99\text{m}}\text{Tc}$ -tetrofosmin (358 ± 177 MBq) and ^{123}I -MIBG (191 ± 29 MBq). This dual-isotope acquisition allowed the simultaneous assessment of cardiac innervation and function. A previous phantom study demonstrated that under simultaneous dual-isotope condition, the presence of ^{123}I did not impact on LVEF assessment within the $^{99\text{m}}\text{Tc}$ energy window for both dedicated CZT cameras (22). In addition, a simultaneous dual-isotope protocol provides a clearer $^{99\text{m}}\text{Tc}$ -tetrofosmin image and a perfect registration to define the heart contours on the $^{99\text{m}}\text{Tc}$ -tetrofosmin image and then accurately measure ^{123}I -MIBG heart uptake (16). As shown in Figure 2, the amount of $^{99\text{m}}\text{Tc}$ activity impacts on $^{99\text{m}}\text{Tc}/^{123}\text{I}$ ratio but does not interfere with the energy resolution of the detector,

modifying only the magnitude but not the width of the photopeak.

Finally, acquisition of both SPECT and planar images using Anger camera usually requires 30-45 min compared with 10 min using CZT cameras, which is much more convenient in patients with heart failure.

Study Limitations

Because of the narrow field of view, the cardiac acquisition does not encompass the upper mediastinum. Consequently, the mediastinal ROI/VOI is positioned in the middle mediastinum on DNM-530c images, while the mediastinal ROI is set on the upper mediastinum when using a conventional Anger camera (7). On the other hand, the size and placement (manual or automated) of the left ventricular ROI does not affect the delayed HMR of ^{123}I -MIBG using conventional planar imaging (8). Therefore, further studies are needed to standardize the placement of the mediastinal ROI or VOI using the different models of available cardiac CZT cameras, at best with standardized HMR using cross-calibrated conversion coefficients (30). Finally, dual-isotope acquisition increases the radiation burden. In this retrospective study, the injected $^{99\text{m}}\text{Tc}$ -tetrofosmin activity was gradually decreased over time as it became clear that CZT camera allows the injection of small amounts of perfusion tracer without compromising image quality.

CONCLUSION

This study demonstrated that determination of late HMR of cardiac ^{123}I -MIBG uptake using dual-isotope (^{123}I and $^{99\text{m}}\text{Tc}$) acquisition on a multi-pinhole CZT camera (DNM-530c) is feasible in patients with heart failure. However, this determination might be performed using transaxial reconstructed images and a linear correction based on phantom data acquisitions.

FINANCIAL SUPPORT

No

DISCLOSURE

Tanguy Blaire: no disclosure

Alban Bailliez: no disclosure

Fayçal Ben Bouallegue: no disclosure

Dimitri Bellevre: no disclosure

Denis Agostini: no disclosure

Alain Manrique: no disclosure

COMPLIANCE WITH ETHICAL STANDARDS

Ethical Approval

All procedures performed in studies involving human participants were in accordance with the ethical standards of the institutional and/or national research committee and with the principles of the 1964 Declaration of Helsinki and its later amendments or comparable ethical standards.

Informed Consent was obtained from all individual participants included in the study.

ACKNOWLEDGMENTS

Amélie Lansiaux, Sylvie Petit, Mathilde Thélu, and the nuclear medicine technicians at Lille for their technical assistance.

REFERENCES

1. Merlet P, Valette H, Dubois-Rande JL, et al. Prognostic value of cardiac metaiodobenzylguanidine imaging in patients with heart failure. *J Nucl Med.* 1992;33:471-477.
2. Nakata T, Miyamoto K, Doi A, et al. Cardiac death prediction and impaired cardiac sympathetic innervation assessed by MIBG in patients with failing and nonfailing hearts. *J Nucl Cardiol.* 1998;5:579-590.
3. Merlet P, Benvenuti C, Moyses D, et al. Prognostic value of MIBG imaging in idiopathic dilated cardiomyopathy. *J Nucl Med.* 1999;40:917-923.
4. Wakabayashi T, Nakata T, Hashimoto A, et al. Assessment of underlying etiology and cardiac sympathetic innervation to identify patients at high risk of cardiac death. *J Nucl Med.* 2001;42:1757-1767.
5. Manrique A, Bernard M, Hitzel A, et al. Prognostic value of sympathetic innervation and cardiac asynchrony in dilated cardiomyopathy. *Eur J Nucl Med Mol Imaging.* 2008;35:2074-2081.
6. Jacobson AF, Senior R, Cerqueira MD, et al. Myocardial iodine-123 metaiodobenzylguanidine imaging and cardiac events in heart failure. Results of the prospective ADMIRE-HF (Adreview Myocardial Imaging for Risk Evaluation in Heart Failure) study. *J Am Coll Cardiol.* 2010;55:2212-2221.
7. Flotats A, Carrio I, Agostini D, et al. Proposal for standardization of 123I-metaiodobenzylguanidine (MIBG) cardiac sympathetic imaging by the EANM Cardiovascular

Committee and the European Council of Nuclear Cardiology. *Eur J Nucl Med Mol Imaging*. 2010;37:1802-1812.

8. Veltman CE, Boogers MJ, Meinardi JE, et al. Reproducibility of planar (123)I-meta-iodobenzylguanidine (MIBG) myocardial scintigraphy in patients with heart failure. *Eur J Nucl Med Mol Imaging*. 2012;39:1599-1608.

9. Sharir T, Ben-Haim S, Merzon K, et al. High-speed myocardial perfusion imaging initial clinical comparison with conventional dual detector Anger camera imaging. *JACC Cardiovasc Imaging*. 2008;1:156-163.

10. Herzog BA, Buechel RR, Katz R, et al. Nuclear myocardial perfusion imaging with a cadmium-zinc-telluride detector technique: optimized protocol for scan time reduction. *J Nucl Med*. 2010;51:46-51.

11. Imbert L, Poussier S, Franken PR, et al. Compared performance of high-sensitivity cameras dedicated to myocardial perfusion SPECT: a comprehensive analysis of phantom and human images. *J Nucl Med*. 2012;53:1897-1903.

12. Verger A, Djaballah W, Fourquet N, et al. Comparison between stress myocardial perfusion SPECT recorded with cadmium-zinc-telluride and Anger cameras in various study protocols. *Eur J Nucl Med Mol Imaging*. 2013;40:331-340.

13. Gimelli A, Liga R, Genovesi D, Giorgetti A, Kusch A, Marzullo P. Association between left ventricular regional sympathetic denervation and mechanical dyssynchrony in phase analysis: a cardiac CZT study. *Eur J Nucl Med Mol Imaging*. 2014;41:946-955.

14. Gimelli A, Liga R, Giorgetti A, Genovesi D, Marzullo P. Assessment of myocardial adrenergic innervation with a solid-state dedicated cardiac cadmium-zinc-telluride camera: first clinical experience. *Eur Heart J Cardiovasc Imaging*. 2014;15:575-585.
15. D'Estanque E, Hedon C, Lattuca B, et al. Optimization of a simultaneous dual-isotope ²⁰¹Tl/¹²³I-MIBG myocardial SPECT imaging protocol with a CZT camera for trigger zone assessment after myocardial infarction for routine clinical settings: are delayed acquisition and scatter correction necessary? *J Nucl Cardiol*. May 25, 2016 [Epub ahead of print].
16. Bellevre D, Manrique A, Legallois D, et al. First determination of the heart-to-mediastinum ratio using cardiac dual isotope (¹²³I-MIBG/^{99m}Tc-tetrofosmin) CZT imaging in patients with heart failure: the ADRECARD study. *Eur J Nucl Med Mol Imaging*. 2015;42:1912-1919.
17. Bocher M, Blevis IM, Tsukerman L, Shrem Y, Kovalski G, Volokh L. A fast cardiac gamma camera with dynamic SPECT capabilities: design, system validation and future potential. *Eur J Nucl Med Mol Imaging*. 2010;37:1887-1902.
18. Bailliez A, Lairez O, Merlin C, et al. Left ventricular function assessment using 2 different cadmium-zinc-telluride cameras compared with a gamma-camera with cardiofocal collimators: dynamic cardiac phantom study and clinical validation. *J Nucl Med*. 2016;57:1370-1375.
19. Inoue Y, Suzuki A, Shirouzu I, et al. Effect of collimator choice on quantitative assessment of cardiac iodine ¹²³I MIBG uptake. *J Nucl Cardiol*. 2003;10:623-632.

20. Verberne HJ, Feenstra C, de Jong WM, Somsen GA, van Eck-Smit BL, Busemann Sokole E. Influence of collimator choice and simulated clinical conditions on ^{123}I -MIBG heart/mediastinum ratios: a phantom study. *Eur J Nucl Med Mol Imaging*. 2005;32:1100-1107.
21. Blaire T, Bailliez A, Ben Bouallegue F, Bellevre D, Agostini D, Manrique A. First assessment of simultaneous dual isotope ($^{123}\text{I}/^{99\text{m}}\text{Tc}$) cardiac SPECT on two different CZT cameras: a phantom study. *J Nucl Cardiol*. Mar 08, 2017 [Epub ahead of print].
22. Blaire T, Bailliez A, Bouallegue FB, Bellevre D, Agostini D, Manrique A. Left ventricular function assessment using $^{123}\text{I}/^{99\text{m}}\text{Tc}$ dual-isotope acquisition with two semi-conductor cadmium-zinc-telluride (CZT) cameras: a gated cardiac phantom study. *EJNMMI Phys*. 2016;3:27-37.
23. Inoue Y, Abe Y, Itoh Y, et al. Acquisition protocols and correction methods for estimation of the heart-to-mediastinum ratio in ^{123}I -metaiodobenzylguanidine cardiac sympathetic imaging. *J Nucl Med*. 2013;54:707-713.
24. Lin LI. A concordance correlation coefficient to evaluate reproducibility. *Biometrics*. 1989;45:255-268.
25. Bland JM, Altman DG. Statistical methods for assessing agreement between two methods of clinical measurement. *Lancet*. 1986;1:307-310.
26. Erlandsson K, Kacperski K, van Gramberg D, Hutton BF. Performance evaluation of D-SPECT: a novel SPECT system for nuclear cardiology. *Phys Med Biol*. 2009;54:2635-2649.

27. Gambhir SS, Berman DS, Ziffer J, et al. A novel high-sensitivity rapid-acquisition single-photon cardiac imaging camera. *J Nucl Med*. 2009;50:635-643.
28. Nakajima K, Okuda K, Matsuo S, et al. Standardization of metaiodobenzylguanidine heart to mediastinum ratio using a calibration phantom: effects of correction on normal databases and a multicentre study. *Eur J Nucl Med Mol Imaging*. 2012;39:113-119.
29. Nakajima K, Okuda K, Yoshimura M, et al. Multicenter cross-calibration of I-123 metaiodobenzylguanidine heart-to-mediastinum ratios to overcome camera-collimator variations. *J Nucl Cardiol*. 2014;21:970-978.
30. Verschure DO, Poel E, Nakajima K, et al. A European myocardial ¹²³I-mIBG cross-calibration phantom study. *J Nucl Cardiol*. Jan 24, 2017 [Epub ahead of print].
31. Takahashi Y, Miyagawa M, Nishiyama Y, Ishimura H, Mochizuki T. Performance of a semiconductor SPECT system: comparison with a conventional Anger-type SPECT instrument. *Ann Nucl Med*. 2013;27:11-16.

FIGURES AND TABLES

FIGURE 1 Imaging study protocol. The first acquisition is a single-isotope planar acquisition, using a conventional camera, whereas the second is a dual-isotope acquisition, using a CZT camera.

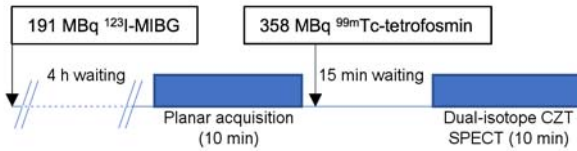


FIGURE 2 Single ^{123}I (24 MBq), single $^{99\text{m}}\text{Tc}$, and simultaneous (^{123}I and $^{99\text{m}}\text{Tc}$) energy spectra using linear sources and DNM-530c. Notice the low tailing effect and the down-scatter of ^{123}I towards $^{99\text{m}}\text{Tc}$ (and the absence of $^{99\text{m}}\text{Tc}$ scatter towards ^{123}I) in the dual-isotope condition, whatever the ratio of $^{99\text{m}}\text{Tc}$: ^{123}I activity; 0.5:1 (A), 1:1 (B), and 5:1 (C) respectively.

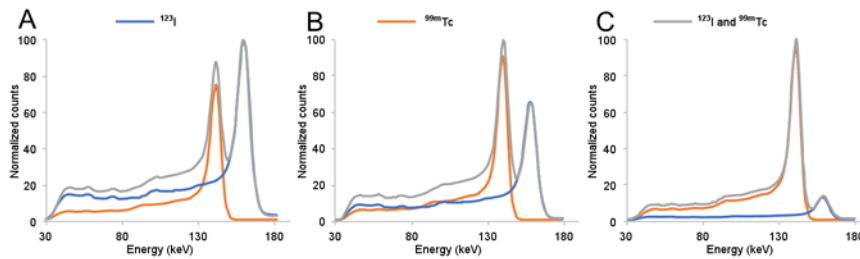


FIGURE 3 Lin's concordance correlation coefficient plots (A, C) and Bland-Atman plots (B, D) showing the agreement between HMR_{reproj} and HMR_{planar} (A, B) and between cHMR_{reproj} and HMR_{planar} (C, D).

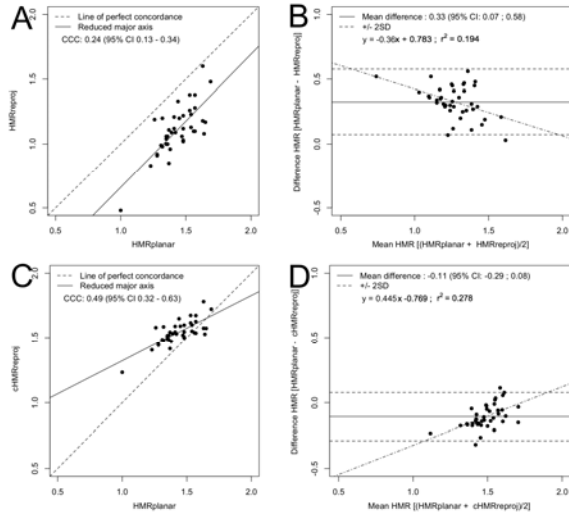


FIGURE 4 Lin's concordance correlation coefficient plots (A, C) and Bland-Atman plots (B, D) showing the agreement between HMR_{transaxial} and HMR_{planar} (A, B; $p < 0.01$) and between cHMR_{transaxial} and HMR_{planar} (C, D)

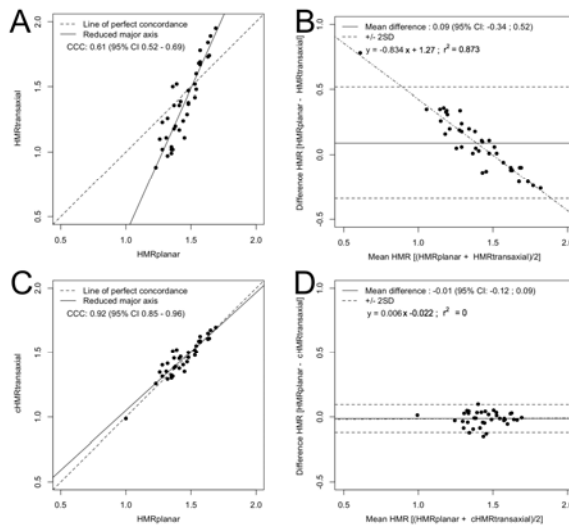


FIGURE 5 Patient #4 with ischemic heart failure (LVEF 44%). HMRs calculated with conventional planar imaging ($HMR_{\text{planar}} = 1.38$, **A**) and using DNM-530c with anterior reprojection images ($HMR_{\text{reproj}} = 0.96$, **E**) and with transaxial reconstructed images ($HMR_{\text{transaxial}} = 1.2$, **C, F**). The ^{99m}Tc image allows positioning on the heart of the ROI (**D**) or the VOI (**B**), and is pasted onto the ^{123}I image (**E** and **C** respectively). Mediastinum VOI on ^{123}I acquisition (**F**). HMR_{reproj} and $HMR_{\text{transaxial}}$ were decreased compared to HMR_{planar} . Lung activity (red arrows) and truncation artefacts (blue arrows) are close to the heart.

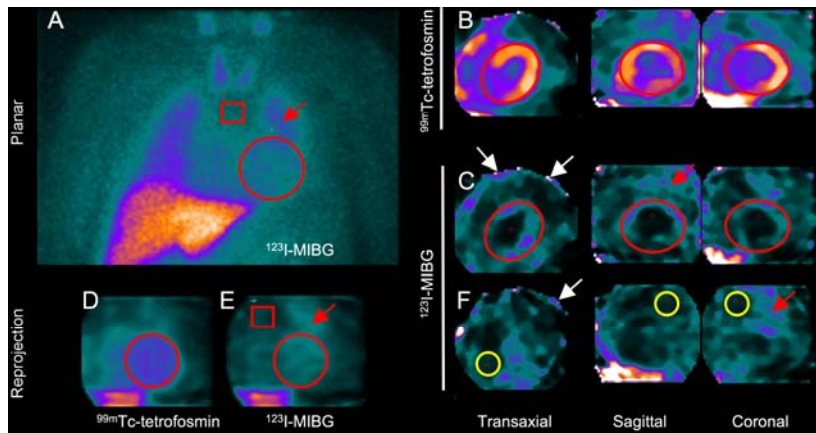


TABLE 1 HMRs from phantom acquisitions

Heart activity (MBq)	HMR _{planar}	HMR _{reproj}	HMR _{transaxial}
1.75	3.56	5.33	6.49
1.5	3.34	4.82	5.77
1.25	2.88	3.84	4.60
1.1	2.77	3.73	4.90
0.94	2.41	2.50	3.81
0.75	2.29	2.14	3.35
0.5	1.86	1.69	2.33
0.35	1.61	1.57	1.65
0.25	1.48	1.34	1.49
0.1	1.21	1.26	0.73
Mean±SD	2.34±0.8	2.82±1.5	3.51±1.94

TABLE 2 Patients characteristics

Case #	Age	Gender	Heart failure	NYHA ¹	LVEF	Administered dose (MBq)		HMR				
						class	(%)	¹²³ I-MIBG	^{99m} Tc-tetrofosmin	Planar	Reproj	Trans
1	70	M	ICM	II	36	196	241	1.54	1.23	1.48	1.6	1.51
2	67	M	ICM	III	20	181	222	1.41	1.12	1.36	1.55	1.46
3	65	F	NICM	II	30	151	264	1.23	0.83	0.88	1.41	1.26
4	77	M	NICM	I	44	125	370	1.38	0.96	1.2	1.48	1.4
5	82	M	NICM	I	44	181	265	1.35	1.04	0.99	1.51	1.31
6	67	M	ICM	II	32	206	282	1.37	0.85	1.18	1.42	1.38
7	79	M	ICM	I	34	212	245	1.53	1.38	1.42	1.68	1.48
8	75	M	ICM	II	33	199	109	1.41	1.21	1.17	1.59	1.38
9	73	M	ICM	II	45	204	632	1.48	1.02	1.47	1.5	1.51
10	78	M	ICM	I	44	186	271	1.39	1.09	1.52	1.54	1.53
11	67	M	NICM	II	40	154	734	1.54	1.13	1.6	1.56	1.56
12	81	M	NICM	II	40	183	276	1.36	1.0	1.5	1.49	1.52
13	69	F	NICM	I	40	192	578	1.48	1.12	1.47	1.55	1.51
14	85	M	ICM	I	40	212	225	1.56	1.1	1.68	1.54	1.59
15	78	M	ICM	I	45	200	176	1.0	0.48	0.22	1.24	0.99
16	64	M	NICM	III	20	189	232	1.57	1.28	1.78	1.63	1.63
17	76	M	ICM	I	36	189	525	1.63	1.18	1.73	1.58	1.61
18	58	M	NICM	III	24	125	370	1.36	1.06	1.02	1.52	1.32
19	70	M	NICM	II	35	119	880	1.63	1.6	1.84	1.79	1.66
20	59	M	ICM	I	35	221	290	1.35	1.00	1.02	1.49	1.32
21	60	M	ICM	II	31	193	549	1.32	0.98	0.97	1.48	1.3
22	82	M	NICM	II	32	175	528	1.65	1.17	1.89	1.58	1.68
23	55	M	NICM	II	35	204	263	1.53	1.26	1.52	1.62	1.52
24	70	M	ICM	II	35	196	288	1.28	0.92	1.23	1.45	1.41
25	77	M	NICM	III	29	191	225	1.48	1.03	1.38	1.51	1.47
26	80	M	ICM	II	30	223	267	1.35	1.06	1.04	1.52	1.33
27	68	M	ICM	II	35	152	263	1.37	1.11	1.36	1.55	1.46
28	80	M	ICM	II	30	188	302	1.32	1.2	1.26	1.59	1.42
29	67	M	NICM	II	33	199	335	1.48	1.22	1.37	1.6	1.47
30	71	M	ICM	II	35	216	308	1.31	0.99	1.11	1.49	1.36
31	70	M	ICM	II	40	214	275	1.26	1.19	1.1	1.58	1.35
32	70	F	NICM	II	33	197	597	1.42	1.09	1.39	1.53	1.47
33	72	F	ICM	I	33	222	235	1.64	1.08	1.74	1.53	1.62
34	54	M	ICM	II	30	181	317	1.44	1.33	1.24	1.65	1.41
35	59	F	NICM	I	42	206	326	1.28	0.91	1.02	1.45	1.32
36	60	F	NICM	I	45	205	377	1.57	1.1	1.69	1.54	1.6
37	72	M	NICM	III	20	247	295	1.45	1.2	1.11	1.59	1.36
38	77	M	NICM	II	32	225	345	1.47	1.06	1.29	1.52	1.43
39	59	M	ICM	II	40	174	294	1.69	1.48	1.95	1.73	1.7
40	59	M	ICM	I	40	198	720	1.57	1.38	1.67	1.68	1.59
Mean	71±				35±9	191±41	358±177	1.44±0.14	1.12±0.19	1.35±0.34	1.54±0.09	1.45±0.14
±SD	9											

¹ New York Heart Association functional class.